coatings

MDPI

Article

Investigation on Fracture Performance of Hot-Mix Asphalt with Reclaimed Asphalt Pavement under Fatigue Loading

Xingren Zhou [1], Weimin Song [2,*] and Hao Wu [2]

[1] Hunan Chajiang Expressway Construction and Development Co., Ltd., 168 North Furong Rd., Changsha 410200, China; 13973173333@163.com
[2] School of Civil Engineering, Central South University, 68 South Shaoshan Rd., Changsha 410075, China; haoutk@csu.edu.cn
* Correspondence: wsong8@csu.edu.cn; Tel.: +86-180-7512-7569

Abstract: Reclaimed asphalt pavement (RAP) has been widely used in asphalt pavement. However, the fatigue performance of hot-mix asphalt (HMA) with RAP is a critical factor to ensure durability. In this study, fatigue tests using an Overlay Tester (OT) were conducted using a novel load-controlled mode. RAP contents were 0, 25% and 50%, respectively. In the cyclic loading, fatigue life and energy parameters were measured. Results indicated that RAP decreased both the fracture energy and tensile strength. Fatigue life was determined using two methods. RAP was proved to be beneficial in prolonging the fatigue life using the two methods at 25 °C. However, opposite conclusions were made about the effect of RAP on fatigue life at −10 °C. At −10 °C, compared to HMA without RAP, the cumulative dissipated energies decreased by 49.1% and 77.3% when RAP contents were 25% and 50%, respectively. At 25 °C, compared to HMA without RAP, the inclusion of 25% RAP increased the cumulative energy by 31.1%, while 50% RAP decreased the cumulative energy by 41.2%. The developments of the dissipated energy and the cumulative energy were consistent with the fatigue life results determined by the first method.

Keywords: fatigue cracking; RAP; fatigue life; dissipated energy; cumulative energy

Citation: Zhou, X.; Song, W.; Wu, H. Investigation on Fracture Performance of Hot-Mix Asphalt with Reclaimed Asphalt Pavement under Fatigue Loading. *Coatings* **2023**, *13*, 1318. https://doi.org/10.3390/coatings13081318

Academic Editor: Valeria Vignali

Received: 4 June 2023
Revised: 24 July 2023
Accepted: 25 July 2023
Published: 27 July 2023

1. Introduction

Asphalt pavement occupies a dominant proportion of pavements around the world. However, the coupled effects of traffic loading and environmental impacts could induce many types of distress, among which fatigue cracking is a major form. For asphalt pavement, fatigue cracking can be classified into two types: top-down cracking and bottom-up cracking [1–3]. The initiation of top-down cracking and bottom-up cracking mainly depends on the thickness of a pavement surface layer. Fatigue cracking is caused by a repeated or fluctuating stress less than the tensile strength of the HMA. In most cases, fatigue cracking is easier to be induced due to the generated stress by repeated traffic loading and environmental factors being lower than the ultimate tensile strength. Fatigue cracking could induce and accelerate the development of other distresses, such as moisture damage, potholes, etc. It is of great significance to investigate the fatigue resistance of hot-mix asphalt (HMA).

The fatigue resistance of a pavement is closely related to the fracture performance of HMA. Generally, due to the viscoelastic nature of asphalt, linear fracture mechanics and elastic-plastic fracture mechanics are adopted at low temperatures and intermediate temperatures, respectively [4,5]. Stress intensity factor and J-integral are used to characterize the fracture roughness in these two scenarios. In addition, fracture energy is also commonly used to characterize the fracture resistance. As asphalt's performance is strongly dependent on temperature, as temperature significantly affects the fracture potential. The effect of material properties on fracture behaviors has been clearly addressed and formulated by many studies. Li et al. [5] conducted statistical analysis on the influential factors

on fracture behaviors of HMA and found that aggregate type and air void content were significant factors. Wang et al. [6] found that crumb rubber (CR)-modified binder could provide better fracture resistance than the unmodified binder. However, there was an optimum CR content (20%) at which the fatigue life was larger. Guo et al. [7] investigated the cracking performance of fiber-reinforced HMA at low temperatures. It was reported that the addition of fiber decreased the moduli and increased the ultimate tensile strain, and improved the fracture toughness. The effects of nano-SiO_2 and nano-calcium carbonate on the fracture performance of HMA were also investigated, and generally, the addition of the nanomaterials enhanced the fracture performance [8,9].

On the other hand, lots of reclaimed asphalt pavements (RAP) are generated during the pavement maintenance and rehabilitation. Due to the increasingly strict environmental regulations, it is a great challenge for authorities to dispose of this type of waste. Stockpiling occupies land and causes environmental pollution. The application of RAP in preparing new HMA has been proved to be a sustainable approach to consuming RAP. On the other hand, RAP contains parts of aged binder and high-quality aggregate. The utilization of RAP in HMA definitely benefits the conservation of natural resources and environmental protection. However, the binder coating RAP aggregate suffers aging for a long time. The aging effect leads to the variation of the chemical composition, leading to the increase in toughness and brittleness of asphalt. Thus, the low cracking temperature of HMA containing RAP is a critical concern for authorities.

Lots of studies have been conducted to evaluate the cracking resistance of HMA with the inclusion of RAP. Song et al. [3] evaluated the effect of RAP on the mode I fracture performance of HMA at both low and intermediate temperatures. Tests indicated that RAP significantly undermined the low-temperature fracture resistance and increased the fracture energy at an intermediate temperature. Although RAP deteriorates fracture resistance, which hinders the widespread use of high-content RAP, some additives could be used to counteract the negative effect of RAP. It should be noted that the effect of RAP on the fracture behaviors of HMA is dependent on the RAP source [10,11]. Obaid et al. [11] found that the RAP source had a significant effect on the fatigue cracking resistance, especially when the RAP content was more than 30%. The addition of rejuvenator could partially improve the fracture resistance due to the softening effect of the rejuvenator on the aged asphalt [3,12]. The blending of RAP binder and virgin binder increased the content of asphaltene, which was proved to have a stronger correlation with MSCR parameters than other indicators [13]. The addition of a rejuvenator could restore the chemical compositions. Besides the rejuvenator, warm-mix techniques were proved to enhance the cracking resistance [14–16], which was ascribed to the fact that warm mix additives lowered the mixing and compaction temperatures, and thus the secondary aging of RAP binder was weakened, which could enhance the performance of HMA. Willis et al. [17] found that the cracking resistance of HMA can be improved by increasing the content of virgin binder when RAP was added; on the other hand, the replacement of the original binder by a softer-grade binder could be beneficial for the cracking potential when RAP was inclusive. Manke et al. [18] found that when the virgin PG 64-22 binder was replaced by a novel bio-derived binder, HMA with 50% RAP could yield satisfactory fracture resistance. Other than rejuvenator, the incorporation of fiber was proved to be a feasible method to enhance the fracture resistance [19,20]. However, the enhancement depends on the fiber type and fiber content. Some other studies were also conducted to investigate the effect of the anti-stripping agent, nanomaterials, and polymer on the cracking resistance of HMA [21,22].

The aforementioned studies were mainly about the fracture performance of HMA with the incorporation of RAP under monotonic loading. Regarding the cracking under fatigue loading, although some methods could be adopted, these tests are indirect methods, or cannot present the crack propagation behaviors. The dissipated creep strain energy ($DCSE_f$) derived from the indirect tensile test (IDT) is an indicator presenting the fatigue performance of HMA [23]. The larger the value of $DCSE_f$, the higher energy restored in

the mixture to resist cracking distress, namely, the better fatigue resistance of the asphalt mixture. The four-point bending test could derive the accurate fatigue life based on the 50% stiffness-reduction method [24,25]. Luo et al. [26] developed a pseudostrain energy approach to accurately characterize the fatigue performance by separating fatigue cracking from permanent deformation in terms of energy consumption. Ozer et al. [1] found that the flexibility index derived from the static IL-SCB test and the fracture energy derived from the static disc-shaped compact tension (DCT) test correlated well with the fatigue life obtained from the accelerated pavement test. Safaei et al. [27] established a relationship between the fatigue of binder and the fatigue performance of HMA using viscoelastic continuum damage modeling. The parameter, $G^*{\cdot}sin\delta$, derived from the dynamic shear rheometer test correlates well with the fatigue performance of a binder. A low $G^*{\cdot}sin\delta$ generally represents a better fatigue performance. Some of the methods aforementioned are indirect, which set up some correlations between indices and fatigue life.

Currently, the overlay tester (OT) is gaining great popularity in characterizing the fracture behaviors of HMA under fatigue loading. The concept of the OT test was first proposed in [28]. Zhou et al. [29] conducted the OT test to detect the crack initiation and propagation under cyclic loading. Results indicated that OT could be used to investigate the fracture potential of HMA under fatigue loading. Wu et al. [2] investigated the cracking resistance of OGFC pavements using OT. The effects of tack coat rate and interface contamination on fatigue cracking were quantificationally explored. Besides the fatigue cracking resistance, OT is also commonly used to reveal the reflective cracking behaviors of HMA [30,31]. However, the fatigue cracking test is conducted using the displacement-controlled model. In this model, the parameter-critical fracture energy, which initiates a crack, is more important than the dissipated energy within each loading cycle. However, the critical fracture energy is sometimes difficult to determine since the maximum load within the loading cycle should be determined first [32]. In the direct tensile load-controlled model, the dissipated energy in each cycle could be directly used to analyze the fracture behaviors, since the specimen withstands continuous tensile loads in both the loading stage and the unloading stage. Therefore, the load-controlled model would be adopted in this study.

The objective of this study is to investigate the fracture behaviors of HMA with different contents of RAP under fatigue loading. Two types of tests, the monotonic test and the fatigue test, were conducted using the OT device. Fatigue loading was applied using a load-controlled model, which was modified from the displacement-controlled model in the original OT test. In the monotonic test, the tensile failure strength and fracture energy were selected to characterize the fracture resistance. In the fatigue test, fatigue life was determined using two approaches: (1) the cycle number at the end of the OT test; (2) the cycle number determined by the 50% modulus reduction method. Dissipated energy in each cycle and the cumulative energy were also adopted to characterize the fatigue damage accumulation.

2. Materials and Methods

2.1. Materials and Mixture Design

In this study, two types of binder were used, including styrene butadiene styrene (SBS) modified binder and RAP binder. The basic properties of the two binders are shown in Table 1. The tests in Table 1 were conducted according to the Chinese Standard (JTGE20-2011, [33]). RAP binder was extracted from RAP using trichloroethylene. The binder content in RAP was determined to be 4.3%. Currently, although scholars investigated the performance of HMA with high RAP content, even up to 100%, the RAP content used in the surface layer is still low. Therefore, RAP contents in this study were 0, 25% and 50%, respectively. For all HMAs in this study, the optimum binder content was 6.2%, which was determined based on the Marshall design method. The complex moduli and phase angles of the blended binder with different contents of RAP binder were presented in Figures 1 and 2. It can be seen that the addition of RAP binder significantly increased the

complex modulus, which was caused by the aging effect of the RAP binder. The larger content of RAP binder, the stiffer the blended binder. The phase angle of the virgin binder (SBS-modified binder) presented a small range of variation, fluctuating around 65° with increasing temperature. This was due to the fact that the cross-linking exists between the SBS modifier and the binder to ensure the viscosity and elasticity of the SBS binder. Thus, there existed a plateau value. The phase angles of the binder with 25% RAP binder were larger than those of the virgin binder at all temperatures. However, for the binder with 50% RAP, when the temperature was no more than 52 °C, the phase angles were lower than those of the virgin binder. From 56 °C, the phase angle difference between binders with 25% RAP and 50% RAP was very slight, and the phase angles increased along with the increase in temperature. The storage modulus and viscous modulus were obtained and shown in Figure 3. It can be seen that at all temperatures, the viscous moduli of the virgin binder with 25% RAP were larger than those of the virgin binder.

Table 1. Basic properties of SBS-modified binder and RAP binder.

Indexes	Unit	Requirement of SBS Binder	SBS	RAP
Penetration (25 °C, 100 g, 5 s)	0.1 mm	30–60	57	43.6
Ductility (5 cm/min, 5 °C)	cm	≥20	47.5	6
Softening point	°C	≥60	82.3	57.3
Kinematic viscosity (135 °C)	Pa·s	≤3.0	1.98	/
Elastic recovery (25 °C, 10)	%	≥75	95	/

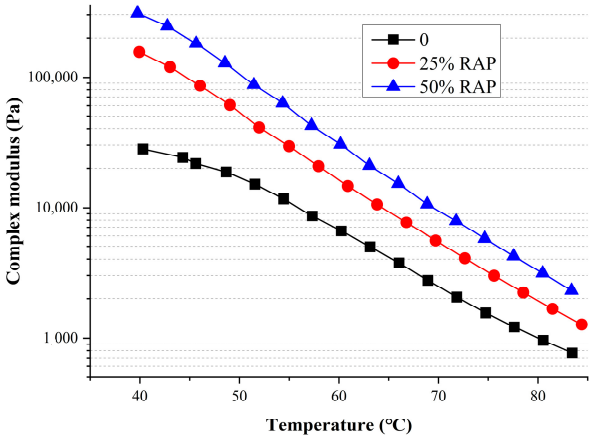

Figure 1. Complex moduli of SBS-modified binder and binders with 25% and 50% RAP.

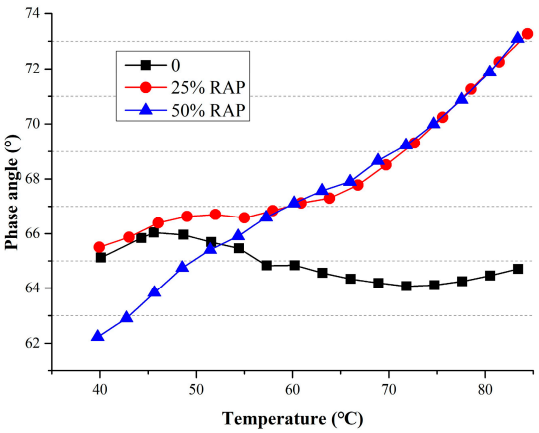

Figure 2. Phase angles of SBS-modified binder and binders with 25% and 50% RAP.

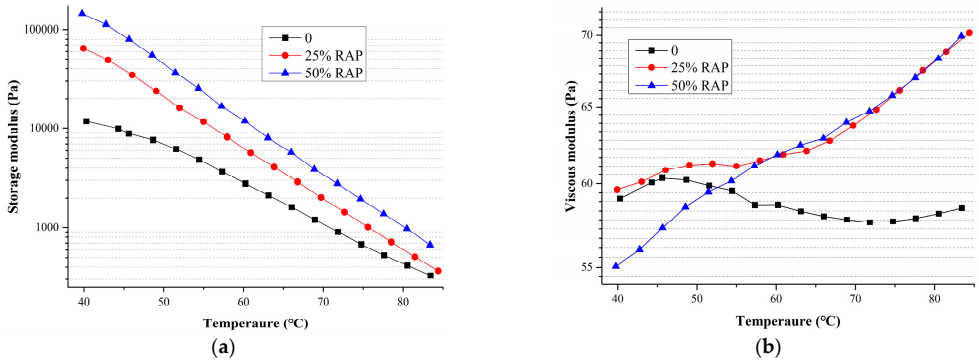

Figure 3. Two parts of the modulus: (**a**) Storage modulus; and (**b**) viscous modulus.

The virgin aggregate and RAP aggregate are both limestones. RAP size varied within the interval between 4.75 and 16 mm. The aggregate gradation, after combining the virgin aggregate and different content of RAP, is shown in Figure 4. The RAP contents selected in this study were 0, 25%, and 50%, respectively.

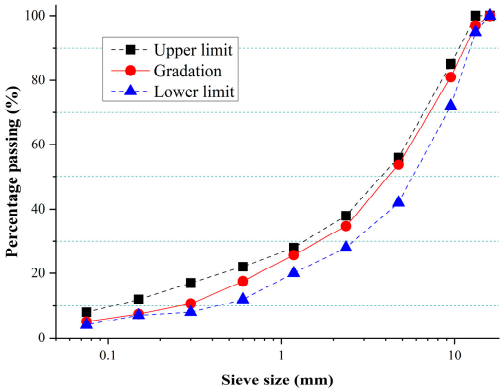

Figure 4. Aggregate gradation of all mixtures.

2.2. Overlay Tester (OT) Setup

To prepare the OT specimen, a Superpave Gyratory Compactor (SGC, Controls, Milano, Italy) was used to compact the cylinder specimen with a diameter of 150 mm and a height of 115 ± 5 mm. The cylinder was then cut to the OT specimen with a length of 150 mm, a width of 76 mm, and a thickness of 38 mm, as shown in Figure 5. Trial compaction was conducted to determine the porosity of the specimen as 4%. The OT specimen was glued to two steel plates. The distance between the two plates was 2 mm. The OT test setup is shown in Figure 6.

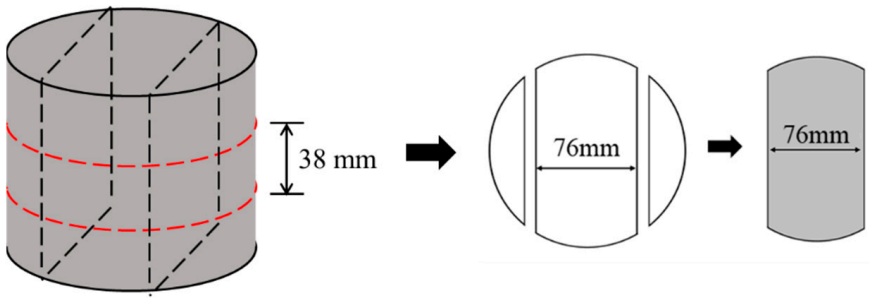

Figure 5. OT specimen preparation.

Figure 6. OT test setup.

Two types of tests were conducted using the OT test devices, the monotonic test and the fatigue test. Before the tests, specimens were cured in an environmental cabinet with the defined temperature for 4 h. In the monotonic test, OT specimens were loaded until fracture failure under a constant rate of 0.5 mm/min. The tensile load was obtained for each type of specimen. Fracture energy was used to characterize the fracture resistance. It was calculated as the ratio between the area underneath the load–displacement curve to the ligament area, as shown in Equation (1). The fatigue test in this study was a modified version of the displacement-controlled test specified in Tex-248-F [34], in which each cycle composes of 5 s loadings and 5 s unloading with the maximum displacement of 0.635 mm. In this study, a sinusoidal stress loading mode with the frequency of 1 Hz at −10 °C and 25 °C was adopted. The cyclic loading was applied using the stress-controlled model with a stress ratio of 0.6, which means the peak load in each cycle was 0.6 times the peak load obtained in the monotonic test (Figure 7). For the monotonic test and fatigue test, triplicate specimens were tested.

$$G = W/A_{lig} \quad (1)$$

where G is the fracture energy (J/mm^2), W is the area underneath the load–displacement curve (J), and A_{lig} is the ligament area of the specimen (mm^2).

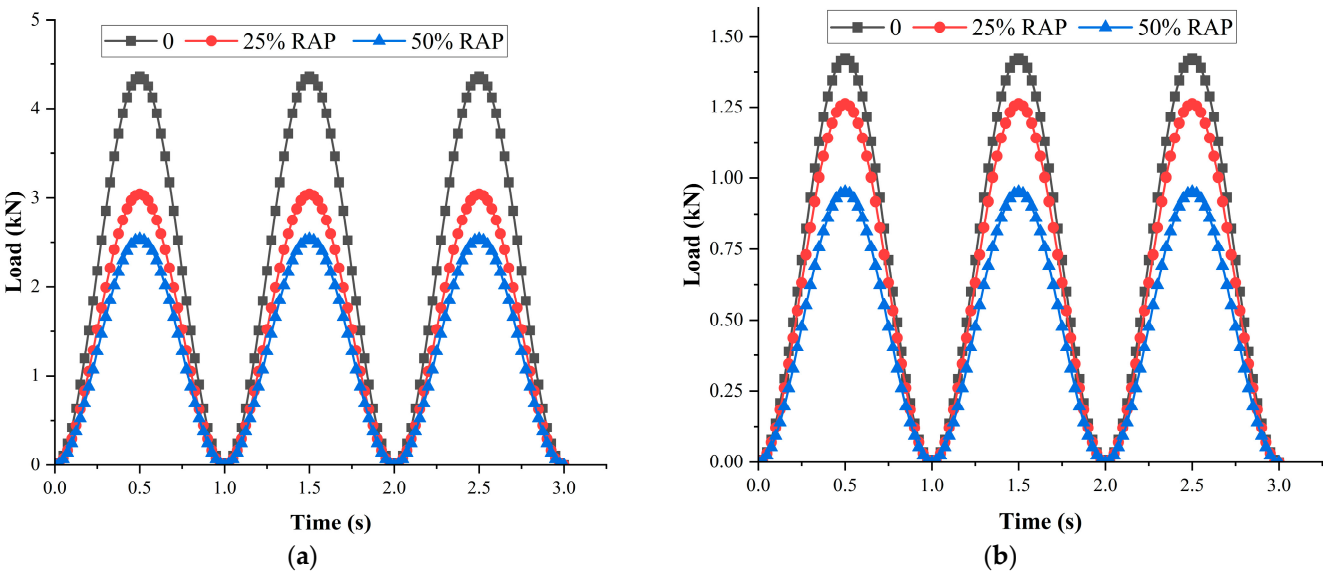

Figure 7. Applied load in fatigue loading: (**a**) −10 °C; (**b**) 25 °C.

To determine the fatigue life, two methods were adopted in this study: (1) the cycle number at the end of the OT fatigue test; (2) the cycle number determined by a 50% reduction in modulus or stiffness [24,35]. The 50% modulus or stiffness reduction method is defined as a 50% decrease in the maximum value of the stiffness or modulus. Some

studies have indicated that the 50% decrease in stiffness or modulus is a valid failure criterion irrespective of the test conditions used [36,37].

3. Results and Discussion

3.1. Monotonic Test Results

OT tensile strength during the monotonic test is shown in Figure 8. The tensile strength was calculated as the ratio between the peak load and the alignment area. It can be clearly observed that due to the visco-elastic behaviors, temperature presented a significant effect on the strength. When the temperature increased from −10 °C to 25 °C, a remarkable reduction in the strength can be seen for each type of specimen. On the other hand, at both −10 °C and 25 °C, the incorporation of RAP significantly deteriorated the tensile behaviors. Compared to the specimens without RAP, 50% RAP decreased the tensile strengths by 41.8% and 33.3% at −10 °C and 25 °C, respectively.

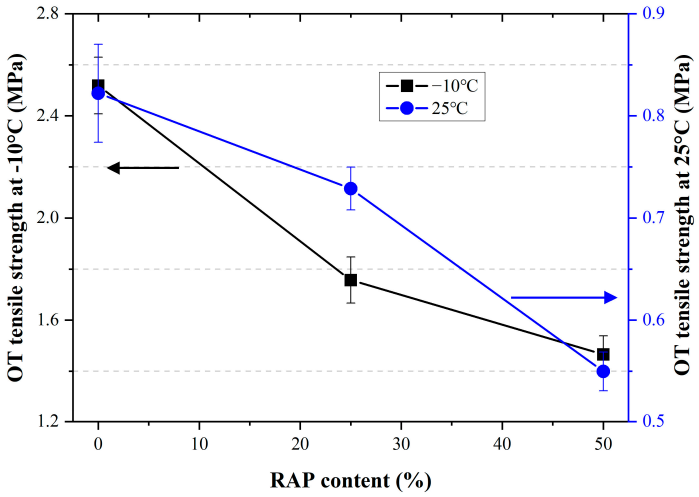

Figure 8. OT failure strength.

Figure 9 presents the facture energies at different temperatures. At the same temperature, the incorporation of RAP significantly decreased the fracture energy, indicating RAP weakened the fracture resistance. Compared to HMA without RAP, 50% RAP reduced the fracture energies by 78.7% and 89.8% at −10 °C and 25 °C, respectively.

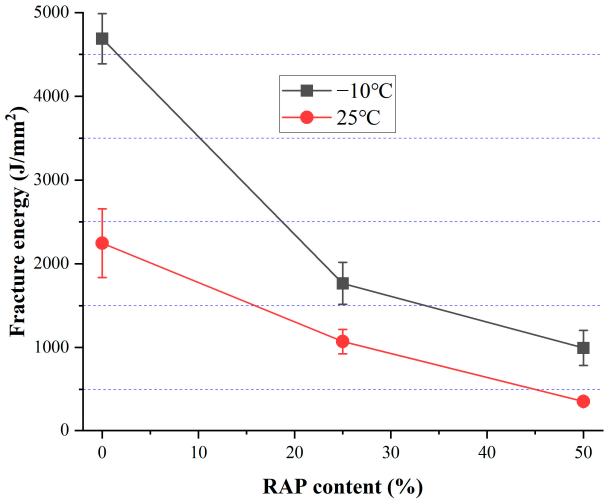

Figure 9. Fracture energy in OT monotonic test.

3.2. Cyclic Loading Test

3.2.1. Fatigue Life

Figure 10 shows the displacement evolution during the cyclic loading. It can be clearly observed that three stages existed in the displacement curves. In the first stage, the displacement increased quickly. The second stage is the stable stage, in which the displacement increased linearly along with the increase in the cycle number; micro-cracking was formed in this stage. In the third stage, micro-cracks propagated and developed into macro-cracks, the displacement increased remarkably and the specimen failed quickly. The durations of the first and third stages were relatively short.

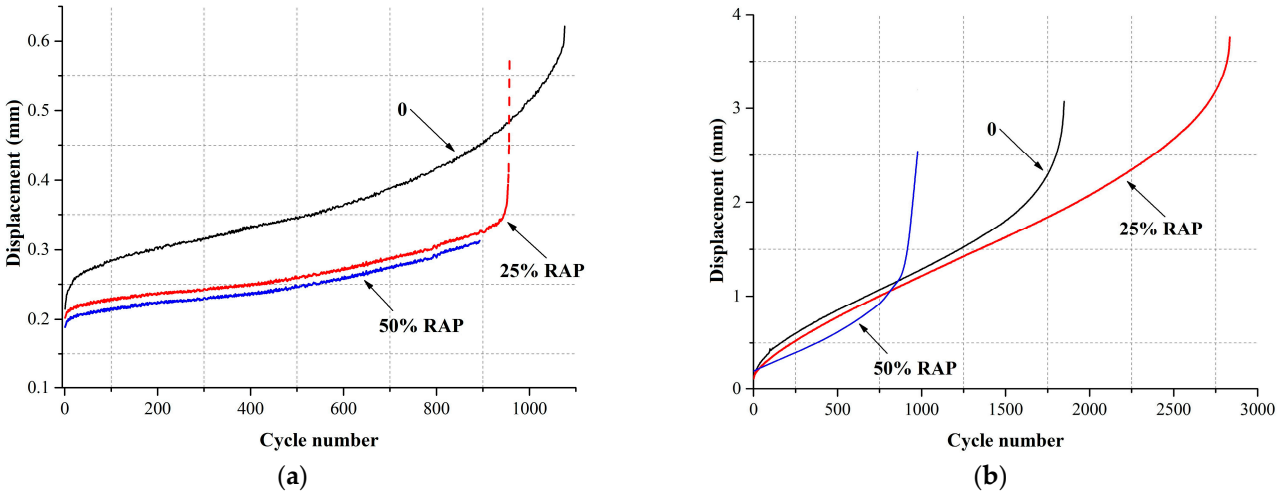

Figure 10. Displacement vs. load cycle at different temperatures: (**a**) −10 °C; (**b**) 25 °C.

When specimens failed, the fatigue life could be determined. The effect of RAP content on the fatigue life can be observed in Figure 11. At −10 °C, when the stress ratio was 0.6, RAP decreased the fatigue life clearly. When RAP content was 50%, fatigue life was reduced by 15.2%. At 25 °C, 25% RAP content increased the fatigue life; when the RAP content increased from 25% to 50%, fatigue life decreased subsequently. However, when the fatigue life was determined by the 50% modulus reduction method, as shown in Figure 12; no matter under −10 °C or 25 °C, the inclusion of RAP could enhance the fatigue resistance. At −10 °C, HMAs with 25% and 50% RAP showed an 11.3% and 4.3% increase in fatigue life in contrast to HMA without the addition of RAP. At 25 °C, 25% and 50% RAP increased the fatigue life by 58.9% and 626.4%, respectively. The difference between Figures 11 and 12 indicated that although the cycle number of HMA without RAP may be larger when the specimen reached failure, the modulus decrease rate of HMA with RAP was lower than the specimens without the inclusion of RAP. It should be noted that data at 25 °C showed a large dispersion. More specimens are suggested to be tested in the future. However, the conclusion can be also drawn that RAP could enhance the fatigue resistance at the intermediate temperature. Zhou et al. [38] also conducted the fatigue test using the SCB test protocol. It was reported that RAP inclusion deteriorated the fatigue performance at both 15 °C and 25 °C, which was slightly different from this study. The result differences between this study and [38] lie in the difference in the basic properties of the binders and the RAP content.

3.2.2. Energy Evolution during the Fatigue Test

The dissipated energy in each cycle and the cumulative dissipated energy were measured to characterize the fracture performance. In the fatigue test, dissipated energy could represent the fatigue damage within each cycle and the cumulative dissipated energy represents the overall fatigue resistance. The larger the cumulative dissipated energy, the better the fracture resistance. Figure 13 shows the load vs. displacement hysteresis loops of

the 1st, 200th, 500th and 1000th loading cycles at −10 °C. The area within the hysteresis loop is the dissipated energy, which represents the difference between the energy provided to the specimen during the loading stage and the energy released during the unloading stage [39]. The dissipated energy could also be obtained using Equation (2). At −10 °C, the monotonic tensile strength decreased as the RAP increased from 0 to 50%, as shown in Figure 8. Therefore, the maximum loads, which were 0.6 times the tensile failure loads, presented obvious differences. In this study, the dissipated energy in each cycle could be obtained by conducting the integration within the loop.

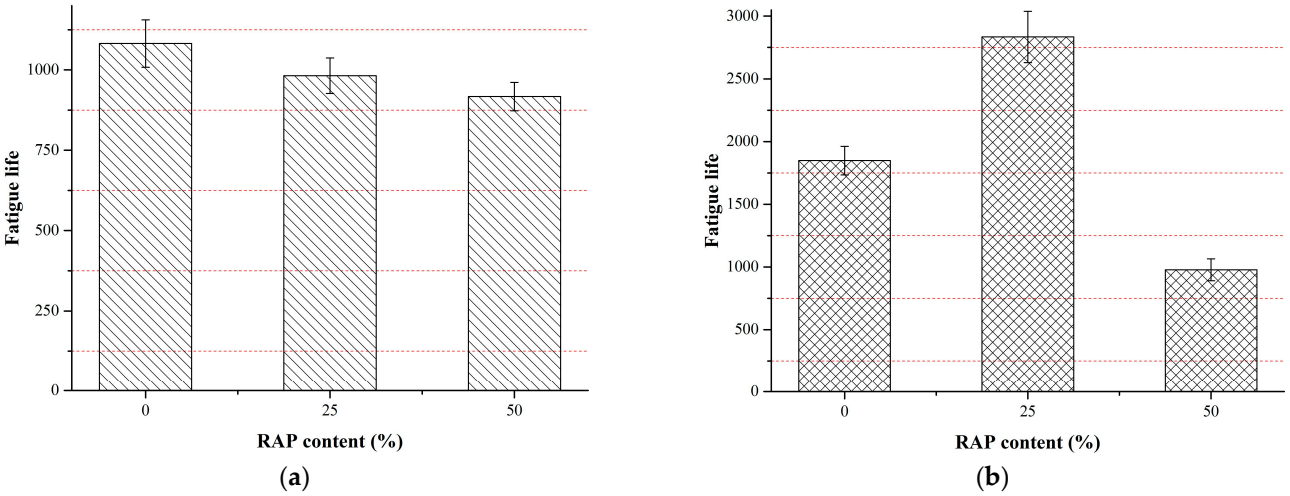

Figure 11. Fatigue life at the end of OT test: (**a**) −10 °C; (**b**) 25 °C.

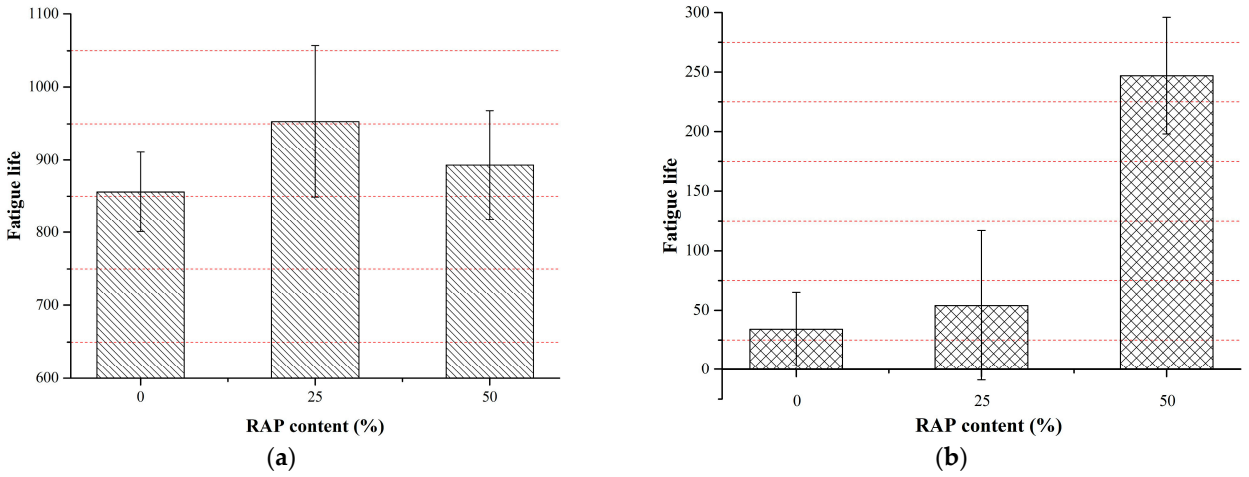

Figure 12. Fatigue life determined by 50% modulus reduction method: (**a**) −10 °C; (**b**) 25 °C.

$$W_i = \pi \sigma_i \varepsilon_i \sin \varphi_i \quad (2)$$

where W_i is the dissipated energy in cycle i (J), σ_i is the stress level in cycle i (Pa), ε_i is the strain level in cycle i, and φ_i is the phase angle in cycle i.

Figure 14 shows the dissipated energy evolution during the fatigue test. At both −10 °C and 25 °C, the dissipated energies of the first few cycles were relatively large, which was possibly caused by the test setup. This stage was of very short duration. With the increase in the cycle number, dissipated energy decreased and increased subsequently. The trend of the dissipated energy was similar to the SCB test results under fatigue loading [39]. In the fatigue test, the increase in displacement was rapid during the first several cycles, which can be seen in Figure 10. Therefore, the loops of the first several cycles may cover a larger displacement range, and then the dissipated energies were larger. At −10 °C, the

inclusion of RAP significantly decreased the dissipated energy in each cycle; the larger the RAP content, the lower the dissipated energy in each cycle. As RAP decreased the dissipated energy in each cycle, the cumulative dissipated energy of HMA without RAP would be larger, indicating more energy would be dissipated during the fatigue test. Therefore, the fracture resistance of HMA without the inclusion of RAP would be superior. At 25 °C, HMA with 25% RAP generated the highest dissipated energy, followed by HMA with 0% and 50% RAP.

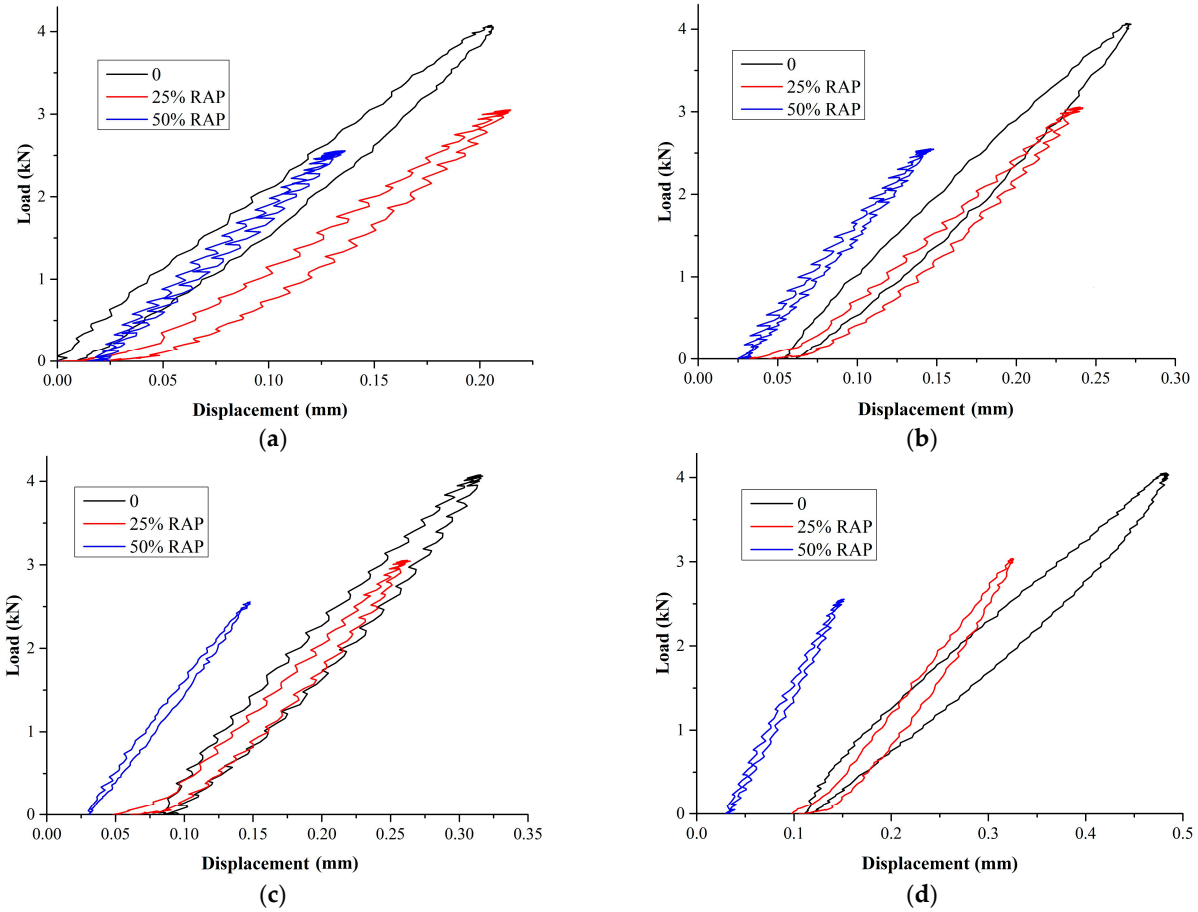

Figure 13. Hysteresis loops at different cycles at −10 °C: (**a**) 1st cycle; (**b**) 200th cycle; (**c**) 500th cycle; and (**d**) 1000th cycle.

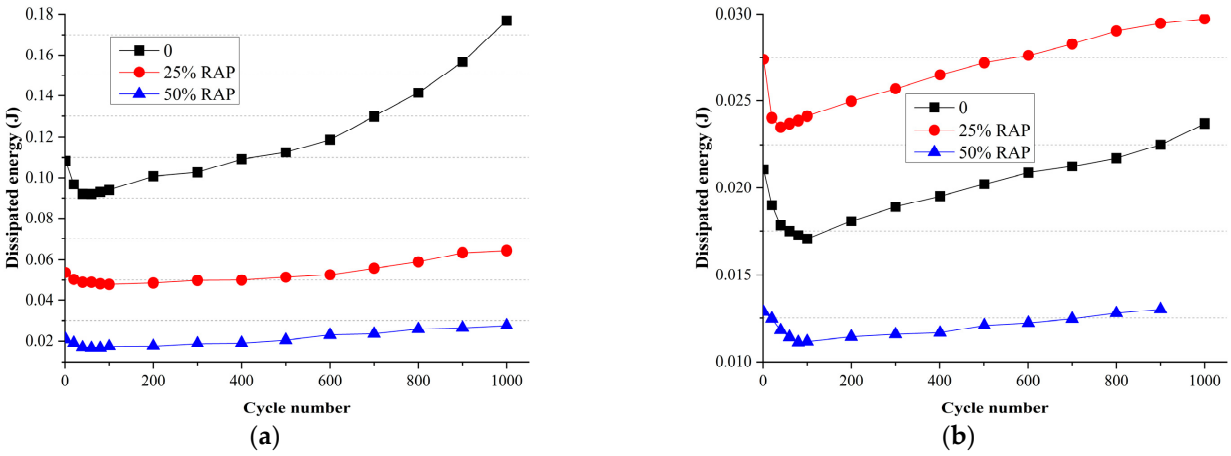

Figure 14. Dissipated energy evolution during the fatigue test: (**a**) −10 °C; (**b**) 25 °C.

The cumulative dissipated energies for all mixtures are shown in Figure 15. Generally, with the increase in the loading cycle, the cumulative energy increased linearly. As the specimen approached failure, the cumulative energy increased more quickly, especially at −10 °C. The slope of the cumulative dissipated energy vs. the cycle number curve represents the increasing rate of the cumulative energy. At −10 °C, the increasing rate of the cumulative energy of HMA without the addition of RAP was larger than other mixtures. The cumulative dissipated energy of HMA without the addition of RAP was also larger, indicating more energy is required for the fatigue failure. With the increase in RAP content, less energy is required. Compared to HMA without RAP, the cumulative dissipated energies decreased by 49.1% and 77.3% when RAP contents were 25% and 50%, respectively. At 25 °C, the energy-increasing rate and the cumulative energy of HMA with 25% RAP was larger. However, when RAP content continued to increase from 25% to 50%, the energy increase rate and the cumulative energy both decreased. Compared to HMA without RAP, the inclusion of 25% RAP increased the cumulative energy by 31.1%, while 50% RAP decreased the cumulative energy by 41.2%. The results indicated that the effect of RAP on the fatigue performance of HMA was strongly dependent on temperature. The results in Figure 15 were consistent with the fatigue life, which was the cycle number at the end of the OT test.

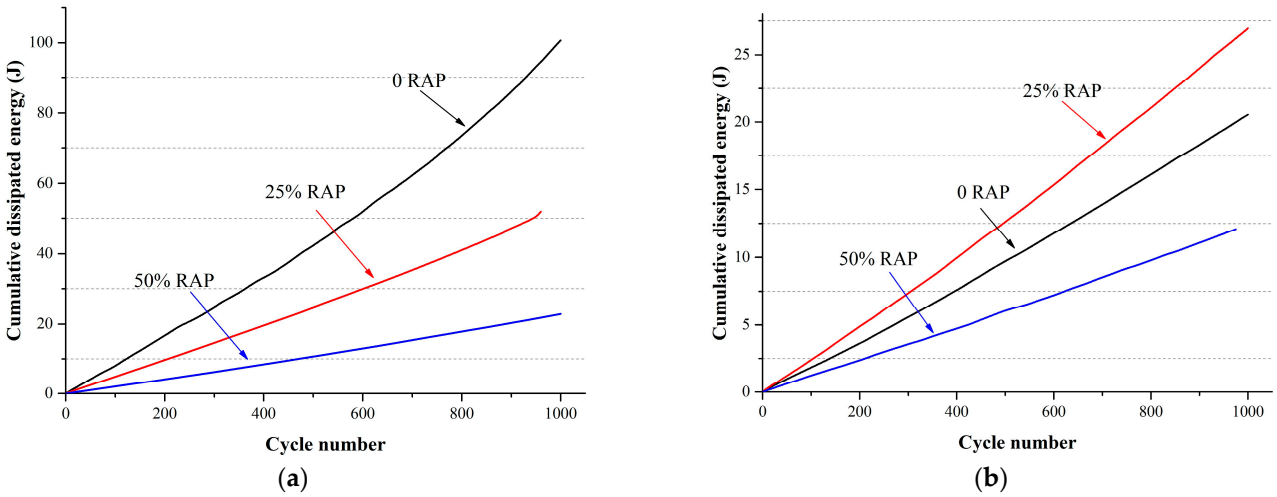

Figure 15. Cumulative dissipated energy: (**a**) −10 °C; (**b**) 25 °C.

Due to the viscoelastic nature of asphalt, the phase angle would be generated between the applied load and the outcoming displacement. Generally, the larger the phase angle, the more viscous the binder. Three stages can be observed in the phase angle evolution curves (Figure 16). A Savitzky–Golay filter [40] was used to process the data and the fitting lines were plotted. During the first stage, the phase angle increased quickly, which may be caused by the heat release during the initial test cycles [41]. The phase angle stably increased during the second stage, corresponding to the stable increase in damage. The last several cycles were within the third stage, in which there existed a sharp increase in the phase angle, corresponding to the quick failure of the specimen. At −10 °C, with the increase in RAP content, the phase angle decreased, indicating that the viscous effect was weakened. At 25 °C, at the same cycle number, the phase angles of HMA with 25% RAP were slightly larger than those of HMA without the inclusion of RAP; and HMA with 50% RAP presented the least phase angles. The results indicated that 25% RAP inclusion made the HMA more viscous at 25 °C, which was caused by the basic properties of the virgin SBS binder and the RAP binder (Table 1). During the fatigue test, the deformation was caused by the viscous effect of the binder. The larger the phase angle, the more viscous the binder. As shown by Equation (2), the dissipated energy of each cycle depends on the phase angle at that cycle; the larger the phase angle, the larger the dissipated energy, and the cumulative

energy would be larger. Figure 2 just shows the phase angles above 40 °C; the results in Figure 16 could be used for the phase angle predictions under low temperatures.

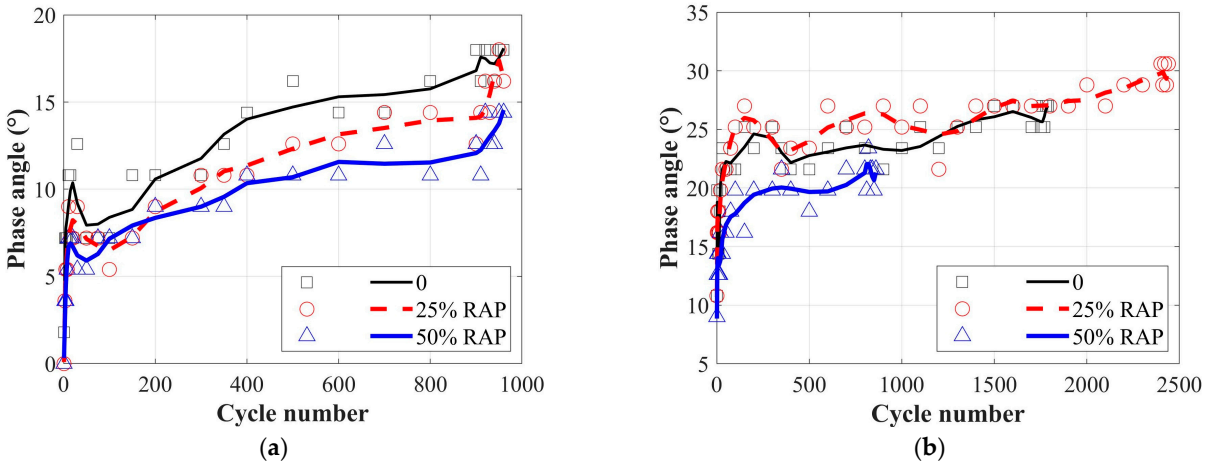

Figure 16. Phase angle evolution during the fatigue test: (**a**) −10 °C; (**b**) 25 °C.

4. Conclusions

This study investigated the fatigue behaviors of HMA with different contents of RAP. Fatigue tests were conducted using the OT device under −10 °C and 25 °C, respectively. Tension monotonic test and load-controlled fatigue test were conducted. Fatigue life, dissipated energy, and cumulative energy were selected to characterize the fatigue resistance of HMA. Based on the results and analysis, the following conclusions can be drawn:

(1) With the increase in RAP content, the monotonic fracture behaviors of HMA, in terms of the fracture strength and fracture energy, were significantly deteriorated at both −10 °C and 25 °C.

(2) Two methods were adopted to determine the fatigue life of HMA with different contents of RAP: the cycle number when the specimen fractured in the OT fatigue test; and the cycle number determined by the 50% modulus reduction method. RAP was proved to be beneficial in prolonging fatigue life using the two methods at 25 °C. However, opposite conclusions were made about the effect of RAP on fatigue life at −10 °C.

(3) At −10 °C, the incorporation of RAP significantly reduced the dissipated energy and the cumulative energy, indicating the fatigue cracking resistance was weakened. At 25 °C, HMA with 25% RAP presented the superior fatigue-cracking resistance in terms of the cumulative dissipated energy. The developments of the dissipated energy and the cumulative energy were consistent with the fatigue life results, determined as the cycle number at the end of the OT test, indicating fatigue life determined by the 50% stiffness reduction method may be not appropriate for fatigue characterization under the constant load-controlled mode.

(4) Fatigue tests under other stress ratios should be conducted in the future. On the other hand, virgin binder and RAP binder with varied properties should be used in the future to further reveal the relationship between phase angle and dissipated energy.

Author Contributions: Conceptualization, X.Z. and W.S.; investigation, X.Z.; methodology, X.Z. and H.W.; writing—original draft, X.Z. and W.S.; writing—review and editing, H.W. All authors have read and agreed to the published version of the manuscript.

Funding: The authors would like to thank the financial support from the National Natural Science Foundation of China (Grant No. 52008405) and Hunan Provincial Natural Science Foundation (Grant No. 2021JJ30845). The contents of this study reflect the views of the authors, who are responsible for the facts and the accuracy of the data presented herein, and do not necessarily reflect any official views or policies.

Institutional Review Board Statement: Not applicable.

Informed Consent Statement: Not applicable.

Data Availability Statement: Data available on request.

Conflicts of Interest: The authors declare no conflict of interest.

References

1. Ozer, H.; Al-Qadi, I.L.; Singhvi, P.; Bausano, J.; Carvalho, R.; Li, X.; Gibson, N. Prediction of pavement fatigue cracking at an accelerated testing section using asphalt mixture performance tests. *Int. J. Pavement Eng.* **2018**, *19*, 264–278. [CrossRef]
2. Wu, H.; Huang, K.; Song, W.; He, F. Characterizing the fatigue cracking behaviors of OGFC pavements using the overlay tester. *Constr. Build. Mater.* **2021**, *307*, 124979. [CrossRef]
3. Song, W.; Gong, H.; Zeng, S.; Cong, L.; Sun, Y.; Wu, H.; Huang, B. Field performance evaluation of open-graded asphalt friction courses: A survival data analysis. *Constr. Build. Mater.* **2021**, *306*, 124745.
4. Saha, G.; Biligiri, K.P. Fracture properties of asphalt mixtures using semi-circular bending test: A state-of-the-art review and future research. *Constr. Build. Mater.* **2016**, *105*, 103–112.
5. Song, W.; Deng, Z.; Wu, H.; Xu, Z. Cohesive zone modeling of I–II mixed mode fracture behaviors of hot mix asphalt based on the semi-circular bending test. *Theor. Appl. Fract. Mech.* **2023**, *124*, 103781. [CrossRef]
6. Wang, H.; Dang, Z.; Li, L.; You, Z. Analysis on fatigue crack growth laws for crumb rubber modified (CRM) asphalt mixture. *Constr. Build. Mater.* **2013**, *47*, 1342–1349. [CrossRef]
7. Guo, Q.; Wang, H.; Gao, Y.; Jiao, Y.; Liu, F.; Dong, Z. Investigation of the low-temperature properties and cracking resistance of fiber-reinforced asphalt concrete using the DIC technique. *Eng. Fract. Mech.* **2020**, *229*, 106951. [CrossRef]
8. Shafabakhsh, G.; Sadeghnejad, M.; Ebrahimnia, R. Fracture resistance of asphalt mixtures under mixed-mode I/II loading at low-temperature: Without and with nano SiO_2. *Constr. Build. Mater.* **2021**, *266*, 120954.
9. Mahani, A.G.; Bazoobandi, P.; Hosseinian, S.M.; Ziari, H. Experimental investigation and multi-objective optimization of fracture properties of asphalt mixtures containing nano-calcium carbonate. *Constr. Build. Mater.* **2021**, *285*, 122876. [CrossRef]
10. Gao, J.; Yang, J.; Yu, D.; Jiang, Y.; Ruan, K.; Tao, W.; Sun, C.; Luo, L. Reducing the variability of multi-source reclaimed asphalt pavement materials: A practice in China. *Constr. Build. Mater.* **2021**, *278*, 122389.
11. Obaid, A.; Nazzal, M.D.; Qtaish, L.A.; Kim, S.S.; Abbas, A.; Arefin, M.; Quasem, T. Effect of RAP Source on Cracking Resistance of Asphalt Mixtures with High RAP Contents. *J. Mater. Civ. Eng.* **2019**, *31*, 04019213. [CrossRef]
12. Song, W.; Zou, X.; Wu, H.; Yang, F. Energy evolution in fracture process of hot mix asphalt containing reclaimed asphalt pavement and rejuvenator. *Theor. Appl. Fract. Mech.* **2023**, *124*, 103809. [CrossRef]
13. Mansourkhaki, A.; Ameri, M.; Habibpour, M.; Shane Underwood, B. Chemical composition and rheological characteristics of binders containing RAP and rejuvenator. *J. Mater. Civ. Eng.* **2020**, *32*, 04020026. [CrossRef]
14. Song, W.; Huang, B.; Shu, X. Influence of warm-mix asphalt technology and rejuvenator on performance of asphalt mixtures containing 50% reclaimed asphalt pavement. *J. Clean. Prod.* **2018**, *192*, 191–198. [CrossRef]
15. Kavussi, A.; Motevalizadeh, S.M. Fracture Failure Evaluation of Foam WMA Mixes Containing RAP by Applying Weibull Probability Distribution Function. *Int. J. Pavement Res. Technol.* **2021**, *15*, 1277–1296. [CrossRef]
16. Kavussi, A.; Motevalizadeh, S.M. Fracture and mechanical properties of water-based foam warm mix asphalt containing reclaimed asphalt pavement. *Constr. Build. Mater.* **2021**, *269*, 121332. [CrossRef]
17. Willis, J.R.; Turner, P.; de Goes Padula, F.; Tran, N.; Julian, G. Effects of changing virgin binder grade and content on high reclaimed asphalt pavement mixture properties. *Transp. Res. Rec.* **2013**, *2371*, 66–73. [CrossRef]
18. Manke, N.D.; Williams, R.C.; Sotoodeh-Nia, Z.; Cochran, E.W.; Porot, L.; Chailleux, E.; Pouget, S.; Olard, F.; Barco Carrion, A.J.D.; Planche, J.-P. Performance of a sustainable asphalt mix incorporating high RAP content and novel bio-derived binder. *Road Mater. Pavement Des.* **2021**, *22*, 812–834. [CrossRef]
19. Ziari, H.; Aliha, M.R.M.; Moniri, A.; Saghafi, Y. Crack resistance of hot mix asphalt containing different percentages of reclaimed asphalt pavement and glass fiber. *Constr. Build. Mater.* **2020**, *230*, 117015. [CrossRef]
20. Yu, B.; Gu, X.; Wu, M.; Ni, F. Application of a high percentage of reclaimed asphalt pavement in an asphalt mixture: Blending process and performance investigation. *Road Mater. Pavement Des.* **2015**, *18*, 753–765. [CrossRef]
21. Khordehbinan, M.; Mahmoud, R. Chemical analysis and middle-low temperature functional of waste polybutadiene rubber polymer modified bitumen. *Pet. Sci. Technol.* **2020**, *38*, 8–17. [CrossRef]
22. Rezaei, S.; Khordehbinan, M.; Fakhrefatemi, S.M.R.; Ghanbari, S.; Ghanbari, M. The effect of nano-SiO_2 and the styrene butadiene styrene polymer on the high-temperature performance of hot mix asphalt. *Pet. Sci. Technol.* **2017**, *35*, 553–560. [CrossRef]
23. Zhao, S.; Huang, B.; Shu, X.; Woods, M. Comparative evaluation of warm mix asphalt containing high percentages of reclaimed asphalt pavement. *Constr. Build. Mater.* **2013**, *44*, 92–100. [CrossRef]
24. Song, W.; Shu, X.; Huang, B.; Woods, M. Laboratory investigation of interlayer shear fatigue performance between open-graded friction course and underlying layer. *Constr. Build. Mater.* **2016**, *115*, 381–389. [CrossRef]
25. Shen, S.; Carpenter, S.H. Application of the dissipated energy concept in fatigue endurance limit testing. *Transp. Res. Rec.* **2005**, *1929*, 165–173. [CrossRef]

26. Luo, X.; Luo, R.; Lytton, R.L. Characterization of fatigue damage in asphalt mixtures using pseudostrain energy. *J. Mater. Civ. Eng.* **2013**, *25*, 208–218. [CrossRef]
27. Safaei, F.; Castorena, C.; Kim, Y.R. Linking asphalt binder fatigue to asphalt mixture fatigue performance using viscoelastic continuum damage modeling. *Mech. Time-Depend. Mater.* **2016**, *20*, 299–323. [CrossRef]
28. Germann, F.P.; Lytton, R.L. *Methodology for Predicting the Reflection Cracking Life of Asphalt Concrete Overlays*; Texas A & M Transportation Institute: Austin, TX, USA, 1979.
29. Zhou, F.; Hu, S.; Chen, D.-H.; Scullion, T. Overlay tester: Simple performance test for fatigue cracking. *Transp. Res. Rec.* **2007**, *2001*, 66–72. [CrossRef]
30. Ma, H.; Zhang, Z. Paving an engineered cementitious composite (ECC) overlay on concrete airfield pavement for reflective cracking resistance. *Constr. Build. Mater.* **2020**, *252*, 119048. [CrossRef]
31. Haslett, K.; Dave, E.; Sias, J.; Linder, E. Statistical Analysis Framework to Evaluate Asphalt Concrete Overlay Reflective Cracking Performance. *Transp. Res. Rec.* **2022**, *2676*, 132–146. [CrossRef]
32. Garcia, V.M.; Miramontes, A.; Garibay, J.; Abdallah, I.; Carrasco, G.; Lee, R.; Nazarian, S. Alternative methodology for assessing cracking resistance of hot mix asphalt mixtures with overlay tester. *Road Mater. Pavement Des.* **2017**, *18*, 388–404. [CrossRef]
33. *JTG E20-2011*; Standard Test Methods of Bitumen and Bituminous Mixtures for Highway Engineering. Research Institute of Highway Ministry of Transport: Beijing, China, 2011.
34. Texas A & M Transportation Institute. TxDOT Designation: Tex–248–F. Test procedure for Overlay Test. In *Construction Division*; Texas A & M Transportation Institute: Austin, TX, USA, 2007.
35. Kim, Y.; Lee, Y.; Lee, H. Correspondence principle for characterization of asphalt concrete. *J. Mater. Civ. Eng.* **1995**, *7*, 59–68. [CrossRef]
36. Lundstrom, R.; Benedetto, H.D.; Isacsson, U. Influence of Asphalt Mixture Stiffness on Fatigue Failure. *J. Mater. Civ. Eng.* **2004**, *16*, 516–525. [CrossRef]
37. Lee, H.J. *Uniaxial Constitutive Modeling of Asphalt Concrete using Viscoelasticity and Continuum Damage Theory*; North Carolina State University: Raleigh, NC, USA, 1996.
38. Zhou, Z.; Gu, X.; Jiang, J.; Ni, F.; Jiang, Y. Fatigue cracking performance evaluation of laboratory-produced polymer modified asphalt mixture containing reclaimed asphalt pavement material. *Constr. Build. Mater.* **2019**, *216*, 379–389. [CrossRef]
39. Isailović, I.; Falchetto, A.C.; Wistuba, M.P. Energy dissipation in asphalt mixtures observed in different cyclic stress-controlled fatigue tests. In Proceedings of the 8th RILEM International Symposium on Testing and Characterization of Sustainable and Innovative Bituminous Materials, Ancona, Italy, 7–9 October 2015; Springer: Dordrecht, The Netherlands, 2015; pp. 693–703.
40. Savitzky, A.; Golay, M.J. Smoothing and differentiation of data by simplified least squares procedures. *Anal. Chem.* **1964**, *36*, 1627–1639. [CrossRef]
41. Diakhaté, M.; Millien, A.; Petit, C.; Phelipot-Mardelé, A.; Pouteau, B. Experimental investigation of tack coat fatigue performance: Towards an improved lifetime assessment of pavement structure interfaces. *Constr. Build. Mater.* **2011**, *25*, 1123–1133.